Title
A Modular Ionophore Platform for Liver-Directed Copper Supplementation in Cells and Animals

Journal
Journal of the American Chemical Society, 140(42)

ISSN
0002-7863

Authors
Su, Timothy A
Shihadih, Diyala S
Cao, Wendy
et al.

Publication Date
2018-10-24

DOI
10.1021/jacs.8b08014

Peer reviewed

JACS
JOURNAL OF THE AMERICAN CHEMICAL SOCIETY
Article
Cite This: J. Am. Chem. Soc. 2018, 140, 13764–13774
pubs.acs.org/JACS

A Modular Ionophore Platform for Liver-Directed Copper Supplementation in Cells and Animals

Timothy A. Su,[†] Diyala S. Shihadih,[‡] Wendy Cao,[†] Tyler C. Detomasi,[†] Marie C. Heffern,[†,#] Shang Jia,[†] Andreas Stahl,[*,‡] and Christopher J. Chang[*,†,§,∥,⊥]

[†]Department of Chemistry, University of California, Berkeley, California 94720, United States
[‡]Department of Nutritional Sciences & Toxicology, University of California, Berkeley, California 94720, United States
[§]Department of Molecular and Cell Biology, University of California, Berkeley, California 94720, United States
[∥]Helen Wills Neuroscience Institute, University of California, Berkeley, California 94720, United States
[⊥]Howard Hughes Medical Institute, University of California, Berkeley, California 94720, United States

Supporting Information

ABSTRACT: Copper deficiency is implicated in a variety of genetic, neurological, cardiovascular, and metabolic diseases. Current approaches for addressing copper deficiency rely on generic copper supplementation, which can potentially lead to detrimental off-target metal accumulation in unwanted tissues and subsequently trigger oxidative stress and damage cascades. Here we present a new modular platform for delivering metal ions in a tissue-specific manner and demonstrate liver-targeted copper supplementation as a proof of concept of this strategy. Specifically, we designed and synthesized an *N*-acetylgalactosamine-functionalized ionophore, Gal-Cu(gtsm), to serve as a copper-carrying "Trojan Horse" that targets liver-localized asialoglycoprotein receptors (ASGPRs) and releases copper only after being taken up by cells, where the reducing intracellular environment triggers copper release from the ionophore. We utilized a combination of bioluminescence imaging and inductively coupled plasma mass spectrometry assays to establish ASGPR-dependent copper accumulation with this reagent in both liver cell culture and mouse models with minimal toxicity. The modular nature of our synthetic approach presages that this platform can be expanded to deliver a broader range of metals to specific cells, tissues, and organs in a more directed manner to treat metal deficiency in disease.

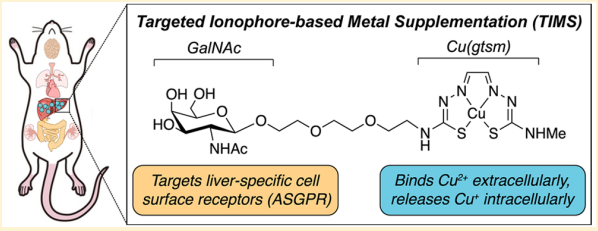

INTRODUCTION

Copper is a required nutrient for all living organisms,[1] enabling fundamental life processes spanning respiration,[2] antioxidant defense,[3,4] neurotransmitter synthesis,[5,6] metabolism,[7,8] and cell signaling.[9−12] Biological copper deficiency hinders these essential functions and correlates with various pathologies including Menkes disease,[13] familial amyotrophic lateral sclerosis,[14,15] neurodegenerative disorders,[16−18] cardiovascular disease,[19,20] and metabolic disorders.[21−27] Current approaches for addressing copper deficiency rely on metal supplementation, often through the administration of copper ionophores, which are molecules that are distinct from copper chelators in that they deliver and release metals into cells rather than sequester and remove metals from cells.[28,29] Conventional copper ionophores include copper complexes with histidine,[30] bisthiosemicarbazones,[31−33] 8-hydroxyquinolines,[16,34] and others.[29] The small and hydrophobic nature of these ionophores, which typically chelate copper in the Cu^{2+} oxidation state, enables their passive diffusion through the cell membrane, after which the reducing intracellular environment acts as a redox trigger for reduction of the metal complex and subsequent Cu^{+} release to copper-binding molecules and proteins (Figure 1A).

Whereas ionophores offer improved cellular copper supplementation relative to the inorganic copper salts typically administered in vitamins, several inherent drawbacks arise from the generic, untargeted nature of copper delivery. First, because copper delivery occurs mostly through a passive transport mechanism, copper delivery into cells is not regulated: for example, if copper supplementation exceeds the buffering capacity of the cytosol, oxidative damage to biomolecules such as DNA, RNA, lipids, and proteins may occur via Fenton-like chemistry.[35] Indeed, copper ionophore supplementation routinely leads to oxidative stress and damage.[36,37] Second, traditional untargeted copper delivery approaches lack tissue specificity.[38,39] As such, if the intent is to treat copper deficiency in a specific organ of interest, such indiscriminate copper delivery will lead to aberrant reactive oxygen species (ROS) generation and oxidative damage in off-target tissues (Figure 1A). To address these challenges, we

Received: July 27, 2018
Published: October 15, 2018

DOI: 10.1021/jacs.8b08014
J. Am. Chem. Soc. 2018, 140, 13764–13774

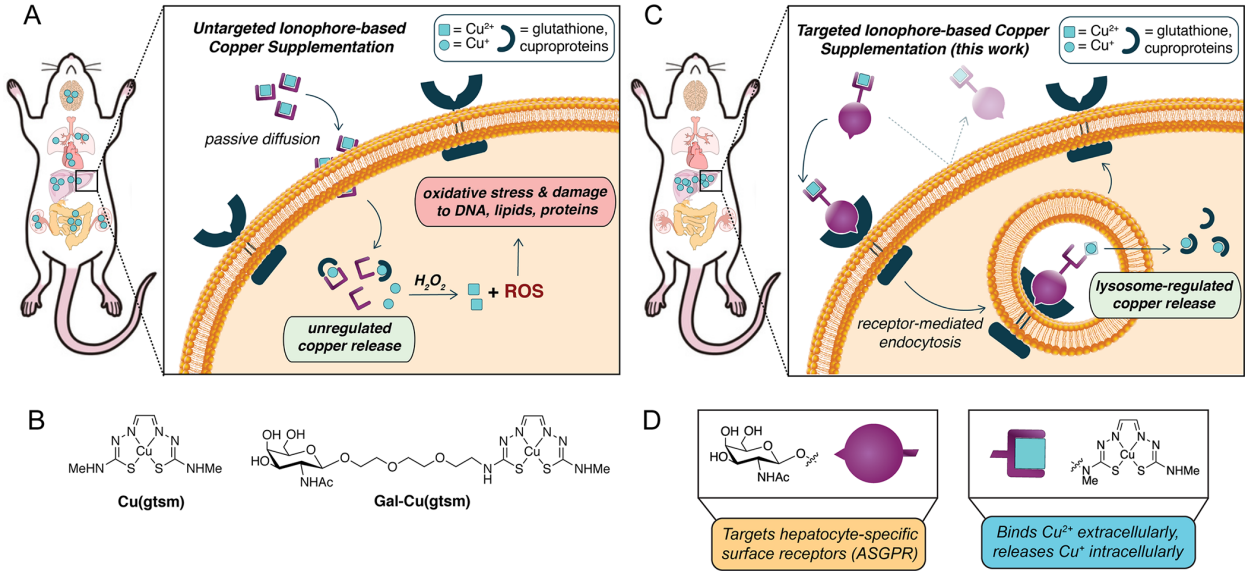

Figure 1. Schematic diagram comparing delivery methods for ionophore-based copper supplementation. (A) Conventional ionophores increase copper levels in many organs due to the nonspecific nature of passive diffusion. For example, Cu(gtsm) releases copper intracellularly following reduction in the cytosolic medium. If too much copper is released such that it exceeds the cell's copper-buffering capacity, excess Cu^{+} can generate reactive oxygen species (ROS) through Fenton-like reactions to induce oxidative stress and damage to the cell. (B) Molecular structures for the untargeted Cu(gtsm) and targeted Gal-Cu(gtsm) ionophores studied here. (C) The targeted ionophore-based metal supplementation (TIMS) strategy presented here enables receptor-mediated metal accumulation with minimal off-target delivery, as shown by liver-selective copper supplementation. The hydrophilicity of the targeted ionophore precludes passive diffusion; ionophore internalization only occurs upon ligand–receptor recognition and endocytosis. Copper release is likely controlled by homeostatic cues at the level of the lysosome to enable regulated copper delivery. (D) The bifunctional ionophore design for Gal-Cu(gtsm) uses a triethylene glycol linker to join the Cu(gtsm) moiety, which binds copper selectively and releases it upon intracellular reduction, with a GalNAc targeting group that is a specific ligand for ASGPR proteins expressed on the cell membranes of hepatocytes.

now present a new, versatile approach to site-specific metal delivery, termed "targeted ionophore-based metal supplementation (TIMS)", which relies on pairing metal-delivering ionophores with targeting ligands that recognize specific cell surface receptors localized to cells and tissues of interest.

We demonstrate the viability of this TIMS approach through the development of a targeted copper supplement that enables selective delivery of copper to the liver in a nontoxic manner owing to interest in addressing hepatic copper deficiency connected to the pathogenesis of nonalcoholic fatty liver disease (NAFLD),[21−23,26,27] which is estimated to afflict 24% of the global population (or 1.8 billion people).[40] NAFLD often leads to severe liver diseases and shows a strong association with cardiovascular diseases, obesity, diabetes, and cancer.[41−43] Indeed, recent work from our laboratories utilized a caged copper luciferin (CCL-1) probe to longitudinally monitor copper levels over the course of NAFLD progression in mice, revealing that hepatic copper deficiency manifests in a diet-induced NAFLD model prior to the formal onset of fatty liver disease. Along these lines, we prepared targeted bifunctional ionophore Gal-Cu(gtsm) and benchmarked its copper delivery properties in cell culture and mice against the untargeted Cu(gtsm) ionophore (Figure 1B). We utilized ICP-MS and bioluminescent imaging techniques to characterize copper supplementation across tissues, observing that the targeted Gal-Cu(gtsm) enables selective hepatic copper supplementation. Furthermore, we utilized a variety of toxicity and histological staining assays to establish that Cu delivery via the TIMS compound is nontoxic, whereas untargeted delivery via passive diffusion incurs significant damage to the liver as well as off-target renal toxicity. Finally, we performed SDS-PAGE and Western blot analysis to characterize expression of copper storage and trafficking proteins, finding that both copper import/export as well as storage proteins are elevated with TIMS treatment. Taken together, this study provides a new type of liver-specific copper supplement and establishes a starting point for the broader use of TIMS reagents as tool compounds to probe the functional roles that metals play in specific cell, tissue, and/or organ types in normal physiology and as directed therapeutic supplements to address metal-deficiency-based pathologies.

RESULTS AND DISCUSSION

Design and Synthesis of a Liver-Targeted Copper Supplement. Figure 1C outlines the TIMS strategy, where (i) ligand–receptor recognition triggers endocytosis and internalization of the receptor–ionophore complex, (ii) the complex releases the metal in the endolysosomal pathway through either intracellular reduction or degradation, and (iii) the metal ion binds to metal storage or trafficking proteins, which can then utilize the metal as needed. In support of this approach, recent studies have shown that the lysosome is a key organelle in dynamic metal regulation,[44−46] and mediating metal delivery through this organelle's homeostatic cues may offer a safer alternative for increasing bioavailable metal ion pools compared to unregulated cytosolic metal release. We note that for this strategy to be effective, the targeted ionophore must be either large or hydrophilic enough to hinder passive diffusion such that metal supplementation is strictly receptor-mediated.

DOI: 10.1021/jacs.8b08014
J. Am. Chem. Soc. 2018, 140, 13764−13774

Scheme 1. Synthetic Route for Accessing Gal-Cu(gtsm)[a]

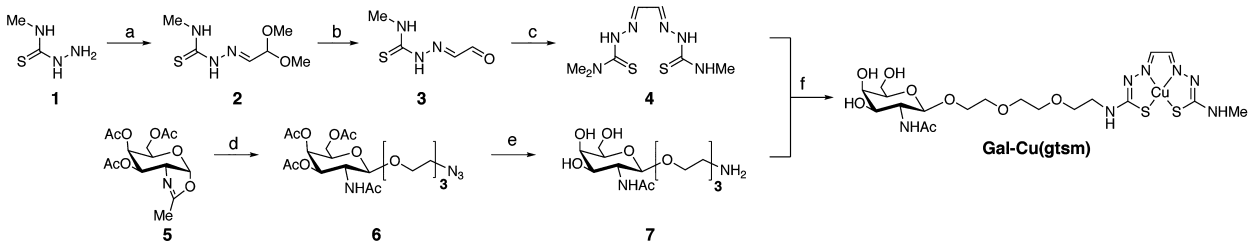

[a]Conditions: (a) 2,2-dimethoxyacetaldehyde, MeOH, rt, quantitative yield; (b) $LiBF_4$, MeCN, H_2O, rt, 81% yield; (c) 4,4-dimethyl-3-thiosemicarbazide, DMF, 4 Å MS, 60 °C, 38% yield; (d) HO-TEG-N_3, TMSOTf, DCE, rt, 81% yield; (e) Pd/C, H_2, MeOH, 92% yield; (f) i. MeCN, 80 °C, 32% yield; ii. $Cu(OAc)_2$, DMF, rt, 73% yield.

With these design principles in mind, we synthesized a bifunctional ionophore that targets the asialoglycoprotein receptor (ASPGR), a C-type lectin membrane receptor that is specifically expressed in the liver at high levels (e.g., ca. 500 000 ASGPR copies per primary hepatocyte[47]), as shown in Figure 1D. We utilized an *N*-acetylgalactosamine (GalNAc) ligand as our targeting group, which binds ASGPR with a K_d value of ca. 10^{-5} M^{-1}.[48] Liver targeting via ASGPR/galactose recognition is a robust strategy that has been used to deliver drugs,[49,50] proteins,[51] siRNA,[52,53] and CRISPR-Cas9;[54] related work has employed metal chelators[55,56] to address copper-excess-based disorders such as Wilson's disease. Although multivalent[47] galactose conjugates offer higher-affinity binding over their monovalent[48,57] counterparts, we decided on the monovalent targeting group in our first-generation design owing to improved atom economy for our payload, a small organometallic complex, as well as for scalable synthesis for longitudinal animal studies.

The design for our TIMS agent is conceptually related to the approach taken for site-specific metal removal, with the key difference being that we attach a targeting group to a metal ionophore rather than a metal chelator.[17,58−60] As such, we paired a GalNAc targeting moiety with the bisthiosemicarbazone complex Cu(gtsm) (Figure 1D), which is a well-established copper ionophore that has been explored as a potential therapeutic for neurodegenerative disorders[31,39,61,62] and cancer.[36,63] The metal-binding and Cu release properties of Cu(gtsm) complex are well-studied and characterized. The gtsm ligand binds Cu^{2+} ($K_d \approx 10^{-18}$ M^{-1}) much more tightly than Cu^{+} ($K_d \approx 10^{-13}$ M^{-1})[64] and releases Cu^{+} upon reduction in the intracellular medium, where it can metalate copper-binding small molecules and proteins.[31,36,65] We reasoned that the significant hydrophilicity conferred by the GalNAc subunit may preclude the ionophore from passive diffusion and encourage receptor-mediated uptake. We chose to link the ionophore and targeting GalNAc ligand with a triethylene glycol chain for enhanced hydrophilicity owing to literature precedent.[50]

Cu(gtsm) was synthesized using literature methods.[66] For Gal-Cu(gtsm), we employed a convergent synthetic approach where we synthesized the ionophore and targeting group fragments independently, then linked them together through a transamination reaction in the penultimate step (Scheme 1).[67,68] Briefly, we installed the glyoxal unit with an acetal protecting group onto thiosemicarbazide **1**, then unmasked acetal **2** with lithium tetrafluoroborate to give iminoacetaldehyde **3**.[69] Condensation with 4,4-dimethyl-3-thiosemicarbazide gave the asymmetrically substituted gtsm analogue **4**. We reacted oxazoline **5**[70] with azidotriethylene glycol in the presence of trimethylsilyl trifluoromethanesulfonate to access the azide-protected peracetylated GalNAc **6**. The azide and O-acetyl groups were deprotected in a single palladium-catalyzed hydrogenation reaction to give GalNAc amine **7**. Transamination between **4** and **7** gave *apo*-Gal-H_2 gtsm, which we then metalated with copper diacetate to give Gal-Cu(gtsm).

Log *P* measurements with a shake-flask octanol−water partition experiment confirmed that Gal-Cu(gtsm) (log *P* = −1.03 ± 0.10) is more hydrophilic than Cu(gtsm) (log *P* = 1.39 ± 0.14).[66,71] Interestingly, we also found that Gal-Cu(gtsm) forms colloids in aqueous buffer with a number-weighted hydrodynamic diameter of 4.60 ± 0.69 nm, whereas Cu(gtsm) does not. Cu(gtsm) and Gal-Cu(gtsm) demonstrate similar Cu−ligand charge transfer absorption band characteristics (Figure S1). We performed further *in vitro* spectroscopic studies to evaluate the stability of Gal-Cu(gtsm) under physiologically relevant conditions. We found that the Gal-Cu(gtsm) complex is stable in aqueous buffers ranging from pH = 3 to 8 (Figure S2). The complex also retains copper selectively in the presence of a 1000-fold excess of Zn^{2+} and Fe^{2+}(Figure S3), which are two other abundant intracellular transition metal ions.[72]

ASGPR-Dependent Copper Delivery in Cell Culture. With the two ionophores in hand, we characterized the behavior of Cu(gtsm) and Gal-Cu(gtsm) in cell lines with high ASGPR expression (HepG2) or no ASGPR expression (HEK 293T). We evaluated ionophore toxicity in these cell lines using propidium iodide staining as a proxy for cell viability, finding that that Cu(gtsm) treatment is toxic at an 8 μM dose in HEK 293T cells, whereas Gal-Cu(gtsm) is nontoxic at a 500 μM dose in both cell lines (Figure S4). We then evaluated the intracellular Cu delivery abilities of the two ionophores using inductively coupled plasma-mass spectrometry (ICP-MS) to analyze total copper levels. We find that Cu(gtsm) elicits dose-dependent increases in cellular copper content for both cell types, whereas Gal-Cu(gtsm) demonstrates a robust dose-dependent copper delivery response only in the ASGPR-expressing HepG2 cells (Figure S5).

Figure 2A,B highlight these differences at an equimolar 4 μM copper dose. We treated HepG2 and HEK 293T cells with either vehicle control, 4 μM Cu(gtsm), or 4 μM Gal-Cu(gtsm) for three hours. Figure 2 displays $^{63}Cu/^{31}P$ ratios from ICP-MS data as a metric for characterizing copper delivery for each treatment condition, with the ^{31}P signal normalizing for number of cells based on cellular phosphate content. Figure 2A shows that Gal-Cu(gtsm) leads to a 4-fold Cu increase relative to the basal levels in HepG2 cells, while Cu(gtsm) treatment

DOI: 10.1021/jacs.8b08014
J. Am. Chem. Soc. 2018, 140, 13764−13774

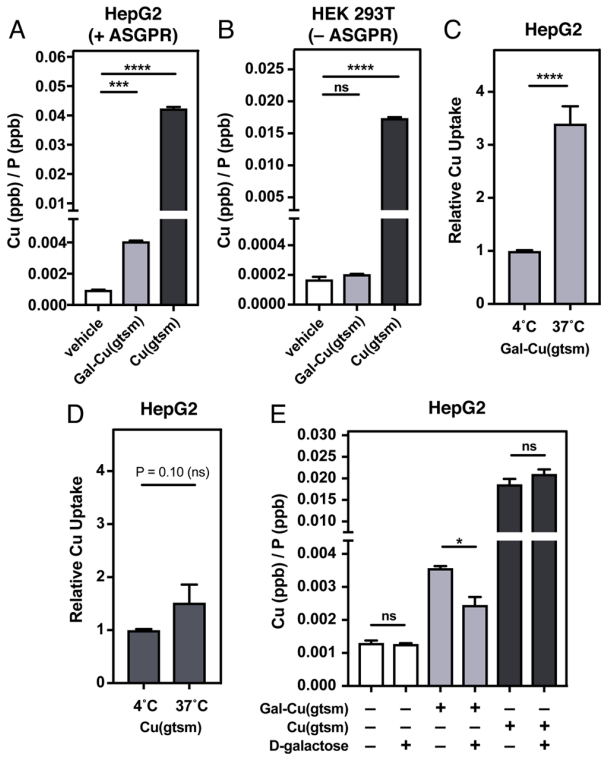

Figure 2. ICP-MS measurements reveal that Cu supplementation via Gal-Cu(gtsm) is ASGPR-dependent. (A) ICP-MS studies comparing Cu levels upon 4 μM Cu-ionophore treatment (0.2% DMSO in serum-free DMEM) over a three-hour time course in HepG2 (ASGPR-expressing) cells. (B) ICP-MS studies upon 4 μM Cu-ionophore treatment (0.2% DMSO in serum-free DMEM) over a three-hour time course in HEK 293T (no ASGPR expression) cells. (C–, D) HepG2 cells were treated with Gal-Cu(gtsm) (20 μM, C) or Cu(gtsm) (4 μM, D) over a one-hour period at either 4 or 37 °C. Data are plotted relative to Cu/P ratio for each ionophore at 4 °C. (E) HepG2 cells were treated with or without D-galactose (1 M in serum-free DMEM) as a competitive ASGPR ligand 15 min prior to treatment with vehicle, Cu(gtsm) (4 μM), or Gal-Cu(gtsm) (20 μM) over a one-hour period. Error bars = SEM (n = 6). Statistical analyses were performed using a one-way ANOVA with Bonferroni's multiple comparisons test (A, B) or a two-tailed Student's t test (C), where *$P \leq 0.05$, ***$P \leq 0.001$, and ****$P \leq 0.0001$.

leads to a 45-fold increase in Cu content. In HEK 293T cells (Figure 2B) that do not express ASGPR, Gal-Cu(gtsm) treatment does not increase cellular copper beyond basal levels, while Cu(gtsm) treatment leads to a 100-fold increase in Cu levels. The data show that Cu(gtsm) delivers copper indiscriminately to both cell types, likely via passive diffusion since Cu(gtsm) is small, hydrophobic, and cell permeable. Conversely, the hydrophilic Gal-Cu(gtsm) experiences limited passive diffusion and does not deliver copper to HEK 293T cells lacking ASGPRs, whereas copper delivery only occurs in the ASGPR-expressing HepG2 cells upon Gal-Cu(gtsm)/ASGPR recognition and internalization.

In support of this mechanistic proposal, we performed temperature-dependent uptake studies at 4 and 37 °C. Gal-Cu(gtsm) demonstrates much higher uptake at 37 °C than at 4 °C, which suggests that Gal-Cu(gtsm)-mediated Cu delivery is an active uptake process (Figure 2C). In contrast, we did not observe any significant differences in Cu delivery ability for Cu(gtsm) between 4 and 37 °C, which suggests that Cu delivery via Cu(gtsm) occurs primarily through a passive diffusion mechanism (Figure 2D). As further support for an ASGPR-mediated Cu delivery mechanism for Gal-Cu(gtsm), we performed a competition experiment where we treated HepG2 cells with vehicle control or ionophore in the presence of D-galactose (1 M) for one hour. The presence or absence of D-galactose does not alter Cu content upon vehicle or Cu(gtsm) treatment in HepG2 cells; however, Cu delivery via Gal-Cu(gtsm) is significantly attenuated in the presence of D-galactose (Figure 2E). We also performed confocal microscopy imaging of HepG2 cells treated with Cu(gtsm) and Gal-Cu(gtsm) using the copper-sensing CF4 fluorescent probe[73] and observed increased fluorescence upon ionophore treatment (Figure S6).

Although the untargeted Cu(gtsm) ionophore delivered more total copper than Gal-Cu(gtsm) under equimolar doses to both HEK 293T and HepG2 cells, the salient finding for expanding the TIMS platform to animal studies was that copper delivery via Gal-Cu(gtsm) occurred exclusively in the ASGPR-expressing HepG2 cells. With these promising cell culture results in hand, we sought to identify whether Gal-Cu(gtsm) could selectively provide Cu supplementation to the liver with minimal off-target delivery in the complex biological milieu of live mice.

Evaluating Liver Target Specificity of Copper Supplementation by Gal-Cu(gtsm) in Living Mice. We chose to characterize liver-targeted copper supplementation in mice because they are common model organisms for elucidating the pathology of metabolic disorders such as NAFLD. Our laboratory recently developed a copper caged luciferin-1 (CCL-1) probe that reports on dynamic changes to the loosely bound, labile Cu^+ pool in transgenic bioluminescent mice (Figure 3A).[27] Here we utilize CCL-1 to characterize liver-directed copper supplementation in the firefly luciferase-expressing FVB-luc$^+$ mouse strain, where luciferase expression enables detection of changes in copper pools throughout the entire mouse. We also imaged ionophore-treated mice with D-luciferin (D-Luc) to normalize the CCL-1 signal and account for CCL-1 cleavage-independent bioluminescent effects. Male FVB-luc$^+$ mice (11–14 weeks old) received intraperitoneal (i.p.) injections of vehicle control, Gal-Cu(gtsm), or Cu(gtsm) at equivalent copper concentrations (0.75 mg Cu/kg mouse). We selected this copper dose based on similar i.p. doses utilized by others to study the therapeutic effects of Cu(gtsm) and its derivatives.[63,74] After six hours, the same mice were anesthetized with isoflurane and given scapular subcutaneous (s.c.) injections of either CCL-1 or D-Luc (0.1 μmol) and imaged with an in vivo imaging system (IVIS) every 5 min over a 40 min period. Representative images of CCL-1-injected mice six hours following vehicle or Gal-Cu(gtsm) treatment are provided in Figure 3B. A full panel of images for CCL-1- and D-Luc-injected mice both 6 and 24 h after ionophore treatment is provided in Figures S7 and S8.

Figure 3C plots the ratio of CCL-1/D-Luc-integrated photon fluxes in the liver region, six hours after ionophore supplementation. We find high increases in liver CCL-1/D-Luc signal ratio responses, suggesting increases in labile copper levels for both the targeted Gal-Cu(gtsm) and Cu(gtsm) compounds. There are two potential factors that may contribute to the observed differences between cell culture and live animal TIMS. First, there is a much higher expression

DOI: 10.1021/jacs.8b08014
J. Am. Chem. Soc. 2018, 140, 13764–13774

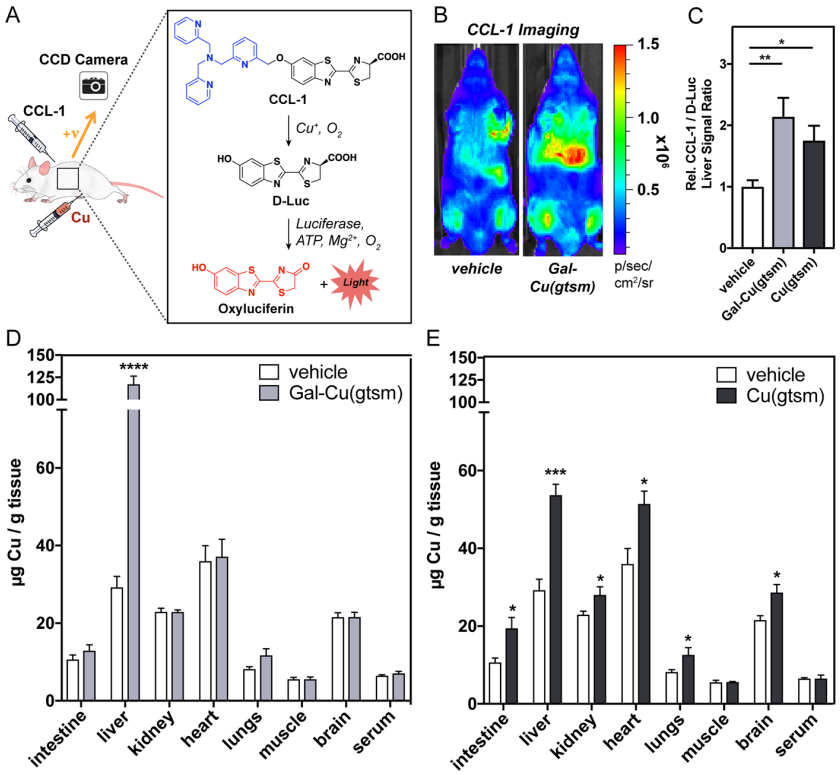

Figure 3. In vivo bioluminescence imaging and ex vivo tissue ICP-MS analysis reveal a tissue-selective increase in hepatic copper stores after Gal-Cu(gtsm) supplementation. (A) Schematic describing Cu^{+}-dependent cleavage of CCL-1 to give bioluminescent signal. Free D-luciferin is released upon binding between Cu and CCL-1, which then interacts with luciferase and emits a photon. (B) Representative images of mice injected s.c. with CCL-1 6 h after vehicle or Gal-Cu(gtsm) i.p. administration. Images for Cu(gtsm)-treated mice are given in Figure S7. (C) Data plotted represent CCL-1 total integrated photon flux as a ratio over D-Luc total integrated photon flux. Total integrated photon flux was collected 5−45 min postinjection in a region of interest drawn over the liver. Liver signal ratio is normalized to vehicle control. Error bars = SEM (n = 5−7). Statistical analysis performed with a one-way ANOVA with Bonferroni's multiple comparisons test where $^{*}P \leq 0.05$. (D, E) Mice were injected i.p. with 0.75 mg equivalent Cu/kg mouse of Gal-Cu(gtsm) or Cu(gtsm) six hours prior to blood and tissue collection. Tissue copper levels relative to tissue wet weight were determined using ICP-MS assays. Error bars = SEM (n = 5). Statistical analyses were performed with a two-tailed Student's t test where $^{*}P \leq 0.05$, $^{***}P \leq 0.001$, $^{****}P \leq 0.0001$.

of ASGPR in primary hepatocytes (ca. 500 000 ASGPR/cell) than in HepG2 cells (ca. 76 000 ASGPR/cell).[47,75] Second, Cu(gtsm) delivery occurs through nonspecific passive diffusion. In cell culture, this property results in high levels of copper delivery. However, in animals, this property leads to nonspecific copper delivery to off-target organs.

The greater propensity for off-target copper accumulation with Cu(gtsm) is supported by *ex vivo* tissue metal analysis via ICP-MS to evaluate total copper levels across organs after Cu(gtsm) and Gal-Cu(gtsm) supplementation at a 0.75 mg Cu/kg dose. We first performed ICP-MS analysis on the stock solutions of Cu(gtsm) and Gal-Cu(gtsm) to confirm that we are indeed administering equivalent copper doses between the ionophores (Figure S9). We collected blood and harvested organs at two different time points (6 h, 24 h) to study the time dependence of copper content and distribution across organs, then processed tissues for ICP-MS analysis. Gal-Cu(gtsm) supplementation results in a 300% increase in liver copper levels after 6 h, with no significant differences in Cu levels in the other extracted organs compared to basal conditions (Figure 3D). Half of this copper is excreted 24 h following Gal-Cu(gtsm) supplementation, with a 150% increase in liver copper relative to basal levels. Interestingly, copper levels in serum and other organs remain at basal levels at 24 h (Figure S10), implying that the supplemented hepatic copper pool is not redistributed from the liver to other organs over time. We find that hepatic copper stores are cleared to basal levels after 72 h (Figure S11).

In contrast, untargeted Cu(gtsm) ionophore treatment leads to a 90% increase in liver copper content at the 6 h time point (Figure 3E), with substantial off-target copper delivery to organs including the intestines, kidney, heart, lungs, and brain. At 24 h, there remains a statistically significant increase in liver, heart, and lung copper relative to basal levels (Figure S10). Although total hepatic copper levels remain substantially elevated at 24 h for both Gal-Cu(gtsm) and Cu(gtsm), interestingly, we find that the bioluminescent CCL-1/D-Luc liver signal returns to basal levels after 24 h (Figure S8). These observations suggest a potential difference in labile copper status at 6 h compared to 24 h, where the delivered copper becomes more tightly sequestered by metal storage proteins at longer time points. Furthermore, we find that the administration of Gal-Cu(gtsm) or Cu(gtsm) offers minimal perturbation to iron and zinc levels across tissues relative to basal conditions (Figures S12 and S13). These data indicate that appending an *N*-acetylgalactosamine moiety to the Cu(gtsm) framework can enable copper supplementation

DOI: 10.1021/jacs.8b08014
J. Am. Chem. Soc. 2018, 140, 13764−13774

selectively to the liver in whole animal settings, likely through an ASGPR-mediated pathway.

Evaluating Toxicity Differences between Targeted Gal-Cu(gtsm) and Untargeted Cu(gtsm) Supplements. Despite the fact that Gal-Cu(gtsm) delivers ca. 4 times more hepatic copper than Cu(gtsm) at an equivalent dose, we find that Gal-Cu(gtsm) treatment is nontoxic, while Cu(gtsm) treatment incurs significant hepatocellular injury, as indicated by liver histology and toxicity assays (Figure 4). Indeed,

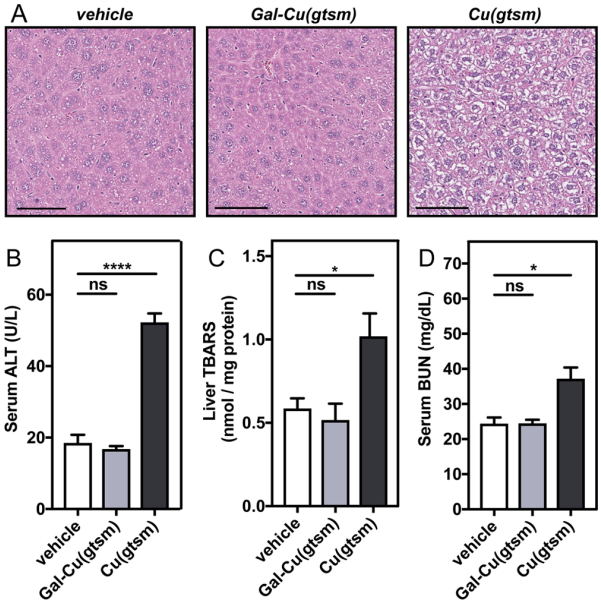

Figure 4. Gal-Cu(gtsm) treatment is nontoxic despite delivering more copper than Cu(gtsm). (A) Representative liver tissue slices from H&E staining show significant hydropic degeneration (wispy/white cytosolic areas surrounding nuclei) upon Cu(gtsm) treatment. Liver sections were isolated six hours following vehicle or 0.75 mg Cu/kg mouse ionophore i.p. injections. Scale bar = 100 μm. (B–D) Toxicity assays were performed on serum (B, D) or liver lysate (C) collected from mice treated with Cu(gtsm) or Gal-Cu(gtsm) at 0.75 mg Cu/kg mouse after 6 h to evaluate liver (B, C) and kidney (D) toxicity. Error bars = SEM (n = 5). Statistical analyses were performed with a one-way ANOVA with Bonferroni's multiple comparisons test where $^*P \leq 0.05$, $^{****}P \leq 0.0001$.

hematoxylin and eosin (H&E) staining on liver tissue slices harvested from mice 6 h after ionophore treatment at 0.75 mg Cu/kg mouse (Figure 4A) show that Gal-Cu(gtsm)-treated liver slices largely resemble those of the vehicle-treated control mice, whereas H&E histology reveals significant hepatocellular damage upon Cu(gtsm) supplementation, with features characteristic of hydropic degeneration that occurs upon acute liver injury (Figure 4A).[78]

To further assess potential ionophore toxicity, we also performed alanine transaminase (ALT) activity and liver thiobarbituric acid reactive substances (TBARS) assays on serum and liver lysate collected from mice treated with Cu(gtsm) or Gal-Cu(gtsm) at the same Cu dose after 6 h (Figure 4B,C). Serum ALT activity assays are commonly used to evaluate hepatocellular injury and evaluate liver health, with increased serum ALT activity indicating potential liver damage. We find virtually the same serum ALT levels for Gal-Cu(gtsm) compared to the vehicle control, but much higher serum ALT levels after Cu(gtsm) treatment (Figure 4B). Likewise, the TBARS assay, which quantifies byproducts such as malondialdehyde generated from lipid peroxidation during oxidative tissue damage, indicates there is significant oxidative-stress-induced liver damage in Cu(gtsm)-treated mice compared to Gal-Cu(gtsm) or vehicle-treated mice (Figure 4C). In both assays, liver health recovers to some extent after 24 h, but there are still significant elevations in ALT activity and TBARS levels relative to basal conditions (Figure S14).

Finally, we investigated off-target toxicity using blood urea nitrogen (BUN) assays, which are commonly elevated under conditions of kidney damage. Figure 4D shows elevated BUN levels for Cu(gtsm), but not for Gal-Cu(gtsm), treatment, which further supports the proposal that targeted copper delivery via Gal-Cu(gtsm) does not promote damage due to off-target copper accumulation. Indeed, previous studies by Cater et al. found significant kidney necrosis occurring upon long-term administration of Cu(gtsm).[36] These studies indicate that targeted copper supplementation via Gal-Cu(gtsm) is nontoxic, whereas untargeted supplementation via Cu(gtsm) incurs hepatic and renal damage.

Selective Upregulation of Copper Trafficking and Storage Proteins as a Mechanism for Minimizing Copper-Induced Toxicity. We speculate that the lack of toxicity resulting from copper supplementation using Gal-Cu(gtsm) compared to its generic nontargeted Cu(gtsm) counterpart originates from their disparate mechanisms for delivery, as hypothesized in Figure 1. In the case of Cu(gtsm) and other conventional copper ionophores, the metal complexes passively diffuse through the cell membrane and release copper upon encountering the reducing cytosolic medium.[65,77] This process is unregulated, and the inability of the cell to buffer such rapid excesses of cytosolic copper likely promotes oxidative stress and damage via Fenton-like chemistry and other redox-mediated pathways. Meanwhile, it is well-established that ASGPR-mediated delivery occurs through clathrin-mediated endocytosis, where ASGPR-ligand recognition is followed by endolysosomal processing.[47] In this case, copper release from Gal-Cu(gtsm) is then compartmentalized and localized to endosomes and lysosomes, in contrast to unregulated Cu^+ release in the cytosol. Importantly, there is mounting evidence that the lysosome is a central organelle for copper storage and homeostasis from algae to mammals.[44,45] Copper delivery via Gal-Cu(gtsm) may then conceivably occur with far greater control, where the lysosome can recruit copper-trafficking proteins in a regulated manner based on homeostatic cues within the cell.[44−46,78]

To test this prediction, we performed Western blot analysis on mouse liver lysates to investigate how these different routes of copper supplementation may affect key players in copper storage and trafficking. Figure 5 shows SDS/PAGE analysis of liver lysates from mice treated with vehicle, Cu(gtsm), and Gal-Cu(gtsm) after 6 or 24 h of treatment at equal protein loading. Expanded blots for all proteins are provided in Figure S15. We first blotted for ATP7B, the major copper export protein in the liver, and found increased ATP7B expression at both time points for Cu(gtsm) and Gal-Cu(gtsm). This observation is consistent with the known role of ATP7B to facilitate the removal of excess hepatic copper via biliary excretion.[46,79] Next, we investigated the expression patterns of CTR1, a copper-trafficking protein that imports copper into the cell from the extracellular matrix and transports copper from the lysosome to the cytosol in concert with CTR2.[45,78]

DOI: 10.1021/jacs.8b08014
J. Am. Chem. Soc. 2018, 140, 13764−13774

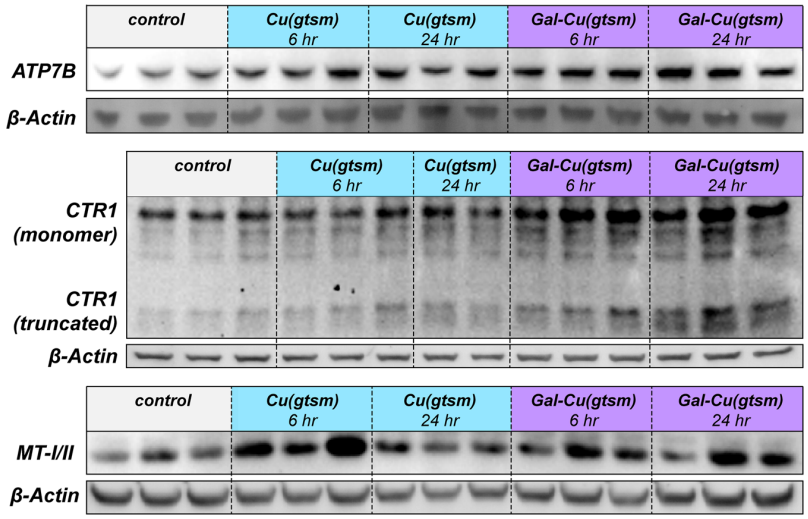

Figure 5. Western blots demonstrate how differences in copper delivery route affect copper storage and trafficking protein expression. SDS/PAGE analysis of liver extracts from mice (n = 2, 3) sacrificed either 6 or 24 h after treatment with vehicle, Cu(gtsm), or Gal-Cu(gtsm) (0.75 mg Cu/kg mouse). Tissues were probed for ATP7B, CTR1, and MT-I/II.

We find increased expression of both the monomer and truncated forms of CTR1 at both 6 and 24 h time points for Gal-Cu(gtsm) supplementation alone. Thiele and co-workers have previously suggested that the truncated CTR1 form may play an important role in copper transport from the lysosome to the cytosol.[78] Because we observe increased CTR1 expression only under conditions of endolysosomal Cu delivery, we hypothesize that CTR1 plays a role in copper transport from the lysosome to the cytosol. Finally, metallothioneins (MTs) are key metal storage proteins in the cytosol. MT-I/MT-II expression increases dramatically upon Cu(gtsm) and Gal-Cu(gtsm) treatment after 6 and 24 h. Blots for the copper chaperone for superoxide dismutase (CCS) did not demonstrate any clear differences between treatment conditions (Figure S15). Further studies are necessary to more conclusively disentangle the relationship between Gal-Cu(gtsm) uptake and lysosomal homeostatic copper regulation and will be the subject of future investigation.

CONCLUDING REMARKS

In this report, we have introduced the concept of targeted ionophore-based metal supplementation, a general strategy to deliver metals in a site-specific manner within living organisms. As an initial proof of concept demonstration of this approach, we synthesized a hepatic copper delivery agent and validated liver-directed copper supplementation in cell culture and mice through *in vivo* bioluminescence imaging and *ex vivo* tissue metal analysis via ICP-MS. We showed that the targeted Gal-Cu(gtsm) ionophore brings far more copper to the liver and minimal Cu to other organs compared to the generic untargeted Cu(gtsm) ionophore. Moreover, receptor-mediated metal supplementation proceeds in a nontoxic manner at the investigated copper dose relative to Cu(gtsm). This work establishes that the TIMS approach is a viable strategy for delivering metal nutrients in a site-specific manner with minimal off-target metal accumulation.

The modular nature of the targeted ionophore building blocks should enable the delivery of other metals and metal-based probes and therapeutics to other organs and sites of interest. We envisage that the TIMS strategy will facilitate both fundamental and therapeutic applications. The site-specific nature of metal delivery may enable us to uncover and elaborate upon the roles that metals play in cellular signaling and function in specific organs of interest at the animal level. As one possible example, Gal-Cu(gtsm) could be used as a tool for studying the complex relationships between copper and lipid signaling in the liver.[25] Likewise, pairing copper ionophores with other tissue-specific targeting groups[80] should further our understanding of the diverse roles that copper plays in different tissue and organ systems.

From a therapeutic perspective, TIMS offers a potential starting point to addressing metal deficiencies in a broad range of diseases with minimal off-target effects. Studies are currently underway in our laboratories to utilize Gal-Cu(gtsm) to study the potential roles and impact of liver-targeted copper supplementation in NAFLD and other metabolic disorders. Gal-Cu(gtsm) may also find potential use in treating hepatocellular carcinomas with minimal off-target effects, as cancer cells demonstrate heightened sensitivity to copper-induced toxicosis.[77,81,82] Beyond the liver, one could use TIMS to address diseases in organs such as adipose tissue, heart, and brain. Indeed, our laboratory recently discovered that dynamic copper binding to PDE3B activates lipolysis in adipose tissue.[12] As such, this TIMS strategy offers a general approach to open new areas for metals in medicine.

EXPERIMENTAL DETAILS

General Synthetic and Characterization Methods. Reactions using air- or moisture-sensitive reagents were conducted in flame-dried glassware under an inert atmosphere of N_2. When dry solvent was required, solvent was passed over activated alumina prior to use. All commercially purchased chemicals were used as received without further purification. 4,4-Dimethyl-3-thiosemicarbazide was purchased from TCI America. All other chemicals and solvents were purchased from Sigma-Aldrich. Cu(gtsm),[66] CCL-1,[27] HO-TEG-N_3,[83] and oxazoline **5**,[70] were synthesized according to previously reported procedures. Silica gel P60 (SiliCycle) was used for column chromatography, and SiliCycle 60 F254 silica gel (precoated sheets, 0.25 mm thick) was used for analytical thin layer chromatography. ^{1}H and ^{13}C NMR spectra were collected at 298 K in deuterated solvents

DOI: 10.1021/jacs.8b08014
J. Am. Chem. Soc. 2018, 140, 13764−13774

from Cambridge Isotope Laboratories (Cambridge, MA, USA) at 25 °C on Bruker AV-300, AVQ-400, AVB-400, AV-500, DRX-500, or AV-600 instruments at the College of Chemistry NMR Facility at the University of California, Berkeley. Chemical shifts for protons are reported in parts per million downfield from tetramethylsilane and are referenced to residual protium in the NMR solvent ($CHCl_3$: δ 7.26; CH_3OH: δ 3.31, DMSO: δ 2.50). Chemical shifts for carbon are reported in parts per million downfield from tetramethylsilane and are referenced to the carbon resonances of the solvent ($CDCl_3$: δ 77.16; DMSO: δ 39.52). Data are represented as follows: chemical shift, multiplicity (s = singlet, d = doublet, dd = doublet of doublets, t = triplet, m = multiplet), coupling constants in hertz, and integration. Low-resolution electrospray mass spectral analyses were performed using an LC-MS (Advion Expression-L Compact MS, ESI source). High-resolution mass spectral analyses (ESI-MS) were carried out at the QB3 Mass Spectrometry Facility at the University of California, Berkeley.

(*E*)-2-(2,2-Dimethoxyethylidene)-*N*-methylhydrazine-1-carbothioamide (2). Synthesis of **2** was adapted from previously reported procedures.[69] 4-Methyl-3-thiosemicarbazide (1.00 equiv, 10.35 g, 98.4 mmol) was added to a 1 L round-bottom flask equipped with a stir bar followed by methanol (500 mL). 2,2-Dimethoxyacetaldehyde (60% wt solution in water) (1.01 equiv, 15.0 mL, 99.43 mmol) was added via syringe, and the resulting solution was stirred overnight, after which a significant white precipitate developed. Volatiles were removed *in vacuo* to yield **2** as a white solid (18.9 g, quantitative yield). ^{1}H NMR (400 MHz, $CDCl_3$): δ 9.20 (s, 1H), 7.37 (s, 1H), 7.04 (d, J = 4.9 Hz, 1H), 4.80 (d, J = 4.9 Hz, 1H), 3.39 (s, 6H), 3.20 (d, J = 4.9 Hz, 3H). ^{13}C NMR (151 MHz, DMSO-d_6): δ 178.28, 140.78, 102.08, 53.44, 30.88. ESI-MS(+): calcd for $C_6H_{13}N_3O_2SNa$ $[M + Na]^+$ m/z 214.1; found 214.6.

(*E*)-*N*-Methyl-2-(2-oxoethylidene)hydrazine-1-carbothioamide (3). Acetal **2** (1.00 equiv, 5.63 g, 29.4 mmol) and lithium tetrafluoroborate (2.00 equiv, 5.52 g, 58.8 mmol) was added to a 2 L round-bottom flask equipped with a stir bar. Acetonitrile (750 mL) was added to the flask, followed by water (15 mL). The reaction mixture was stirred at room temperature for 6 h, during which the reaction mixture transformed from a neon yellow to orange color. The reaction mixture was concentrated, then diluted with ethyl acetate (300 mL). The organic layer was washed with saturated $NaHCO_3$ (50 mL), water (50 mL), and brine (50 mL), dried over Na_2SO_4, filtered, and then concentrated *in vacuo*. The resulting brown solid was sonicated and extracted with hexane/ethyl acetate, 1:1, v/v (400 mL), then filtered. The filtrate was concentrated *in vacuo* to obtain **3** as an orange powder (3.41 g, 81% yield). ^{1}H NMR (600 MHz, DMSO-d_6): δ 12.24 (s, 1H), 9.46 (d, J = 7.8 Hz, 1H), 9.00 (d, J = 5.7 Hz, 1H), 7.44 (dd, J = 7.8, 1.1 Hz, 1H), 3.01 (d, J = 4.6 Hz, 3H). ^{13}C NMR (151 MHz, DMSO): δ 191.30, 178.33, 138.58, 39.52, 31.17. ESI-MS could not be obtained.

(*E*)-*N*,*N*-Dimethyl-2-((*E*)-2-(2-(methylcarbamothioyl)-hydrazinylidene)ethylidene)hydrazine-1 Carbothioamide (4). Compound **3** (1.00 equiv, 1.70 g, 11.71 mmol), 4,4-dimethyl-3-thiosemicarbazide (1.05 equiv, 1.47 g, 12.30 mmol), activated 4 Å MS, and DMF (50 mL) were added to a 100 mL round-bottom flask equipped with a stir bar and condenser. The reaction mixture was stirred at 60 °C overnight under nitrogen to yield a dark brown solution. The reaction mixture was filtered to remove sieve dust and other particulates, then distilled to remove dimethylformamide (DMF). The resulting crude brown solid was sonicated and washed with ethanol (3 × 20 mL) and methanol (1 × 3 mL) to yield **4** as a beige powder (1.08 g, 38% yield). Subsequent filtrate precipitation at −20 °C yielded additional material albeit of reduced purity. ^{1}H NMR (400 MHz, DMSO-d_6): δ 11.67 (s, 1H), 11.18 (s, 1H), 8.42 (d, J = 4.8 Hz, 1H), 7.88 (d, J = 8.5 Hz, 1H), 7.74 (d, J = 8.5 Hz, 1H), 3.25 (s, 6H), 2.97 (d, J = 4.5 Hz, 3H). ^{13}C NMR (101 MHz, DMSO): δ 180.11, 177.54, 142.26, 140.66, 41.94, 39.52, 30.94. ESI-MS(−): calcd for $C_7H_{13}N_6S_2$ $[M - H]^-$ m/z 245.1; found 245.2.

(2*R*,3*R*,4*R*,5*R*,6*R*)-5-Acetamido-2-(acetoxymethyl)-6-(2-(2-(2-azidoethoxy)ethoxy)ethoxy)tetrahydro-2*H*-pyran-3,4-diyl-diacetate (6). Compound **5** (1.00 equiv, 3.3 g, 10.02 mmol), HO-TEG-N_3 (1.10 equiv, 1.93 g, 11.00 mmol), and dichloroethene (DCE) (60 mL) were added to a 200 mL round-bottom flask followed by a scoop of activated 4 Å molecular sieves. After stirring for 5 min, trimethylsilyl trifluoromethanesulfonate (0.50 equiv, 0.91 mL, 5.01 mmol) was added via syringe to the reaction mixture and stirred overnight. The reaction mixture was filtered, and the filtrate was washed with a saturated sodium bicarbonate solution. The organic layer was dried with Na_2SO_4, filtered, concentrated *in vacuo*, and then purified with silica gel chromatography (ethyl acetate to 9/1 ethyl acetate/methanol) to yield **6** as a pale orange oil (3.65 g, 72% yield). ^{1}H NMR (600 MHz, $CDCl_3$): δ 6.14 (d, J = 9.3 Hz, 1H), 5.32 (dd, J = 3.4, 1.1 Hz, 1H), 5.05 (dd, J = 11.2, 3.4 Hz, 1H), 4.78 (d, J = 8.6 Hz, 1H), 4.22 (dt, J = 11.2, 8.9 Hz, 1H), 4.19−4.10 (m, 2H), 3.93−3.83 (m, 3H), 3.76−3.65 (m, 4H), 3.63 (dd, J = 7.1, 3.2 Hz, 4H), 3.51−3.39 (m, 2H), 2.15 (s, 3H), 2.04 (s, 3H), 1.99 (s, 3H), 1.98 (s, 3H). ^{13}C NMR (151 MHz, $CDCl_3$): δ 170.54, 170.42, 170.39, 170.29, 102.15, 71.56, 70.82, 70.64, 70.56, 70.32, 69.72, 68.51, 66.65, 61.50, 50.73, 50.47, 23.12, 20.68, 20.62, 20.61. ESI-MS(+): calcd for $C_{20}H_{32}N_4NaO_{11}$ $[M + Na]^+$ m/z 527.2, found 527.7.

***N*-((2*R*,3*R*,4*R*,5*R*,6*R*)-2-(2-(2-(2-Aminoethoxy)ethoxy)-ethoxy)-4,5-dihydroxy-6-(hydroxymethyl)tetrahydro-2*H*-pyran-3-yl)acetamide (7).** Compound **6** (1.00 equiv, 1.36 g, 2.70 mmol) was added to a 100 mL round-bottom flask equipped with a stir bar and dissolved in methanol (15 mL). Palladium (10%) on activated carbon (∼50 mg) was slowly added to the flask, which was subsequently placed under vacuum and backfilled with hydrogen gas three times. The reaction mixture was stirred under a hydrogen gas balloon for 20 h. The reaction mixture was filtered over Celite, which was then rinsed with methanol (40 mL). The filtrate was concentrated to yield **7** as a pale yellow semisolid (0.88 g, 92% yield), which was then carried forward to the next step. ^{1}H NMR (500 MHz, CD_3OD): δ 4.39 (d, J = 8.4 Hz, 1H), 4.01−3.87 (m, 2H), 3.83 (d, J = 3.4 Hz, 1H), 3.80−3.54 (m, 12H), 3.49 (t, J = 6.2 Hz, 1H), 2.91 (t, J = 5.3 Hz, 1H), 1.98 (s, 3H). ^{13}C NMR (151 MHz, MeOD): δ 170.38, 103.55, 76.62, 73.00, 71.32, 71.21, 71.00, 70.81, 69.92, 69.64, 62.52, 53.94, 49.58, 23.16. ESI-MS(+): calcd for $C_{14}H_{29}N_2O_8$ $[M + H]^+$ m/z 353.2, found 353.4.

***apo*-Gal-H_2 gtsm.** Compound **4** (1.00 equiv, 0.56 g, 2.27 mmol), compound **7** (1.10 equiv, 0.88 g, 2.50 mmol), and acetonitrile (100 mL) were added to a 250 mL round-bottom flask equipped with a reflux condenser and stir bar. The reaction mixture was refluxed at 82 °C overnight, in which the reaction mixture turned from a light orange to brown color. The reaction mixture was cooled to room temperature, and Celite (10 g) was added to the flask. The contents were then concentrated *in vacuo*. The crude material loaded onto Celite was subjected to flash silica gel chromatography (100% dichloromethane (DCM) to 9/1 DCM/MeOH to 4/1 DCM/MeOH gradient) to afford *apo*-Gal-H_2 gtsm as a beige solid (436 mg, 32% yield). ^{1}H NMR (400 MHz, DMSO-d_6): δ 11.80 (d, J = 18.1 Hz, 2H), 8.51 (d, J = 4.7 Hz, 1H), 8.43 (t, J = 5.8 Hz, 1H), 7.73 (s, 2H), 7.61 (d, J = 9.0 Hz, 1H), 4.62−4.55 (m, 3H), 4.50 (d, J = 4.3 Hz, 1H), 4.28 (d, J = 8.4 Hz, 1H), 3.78 (dt, J = 10.1, 4.2 Hz, 1H), 3.74−3.62 (m, 5H), 3.61−3.38 (m, 15H), 3.32−3.23 (m, 1H), 2.96 (d, J = 4.5 Hz, 3H), 1.80 (s, 3H). ^{13}C NMR (101 MHz, DMSO-d_6): δ 177.57, 177.05, 169.63, 140.51, 140.00, 101.40, 75.36, 71.66, 69.81, 69.66, 68.30, 67.67, 67.60, 60.55, 52.03, 43.15, 39.52, 30.99, 23.17. ESI-MS(−): calcd for $C_{19}H_{34}N_7O_8S_2$ $[M - H]^-$ m/z 552.2; found 552.4.

Gal-Cu(gtsm). Compound **8** (1.00 equiv, 0.24 g, 0.43 mmol) and copper acetate (1.02 equiv, 87 mg, 0.44 mmol) were added to a 25 mL round-bottom flask equipped with a stir bar. Anhydrous DMF (4.7 mL) was added, and the reaction mixture immediately adopted a crimson red color. The resulting solution was stirred at room temperature overnight. The reaction mixture was concentrated *in vacuo*, and ethanol (2.5 mL) was added to precipitate a dark red solid, which was then frit filtered and rinsed with ethanol (2.5 mL) and diethyl ether (2 × 5 mL), giving Gal-Cu(gtsm) as a dark red powder (192 mg, 73% yield). High-resolution ESI-MS(+): calcd for $C_{19}H_{34}CuN_7O_8S_2$ $[M + H]^+$ m/z 615.1201, found 615.1202.

Cell Culture Procedures. Cells were maintained by the UC Berkeley Tissue Culture Facility. HEK 293T and HepG2 cells were

DOI: 10.1021/jacs.8b08014
J. Am. Chem. Soc. 2018, 140, 13764−13774

maintained as a monolayer in exponential growth at 37 °C in a 5% CO_2 atm. HEK 293T cells were maintained in Dulbecco's modified Eagle medium (DMEM, Gibco) supplemented with 10% fetal bovine serum (FBS, Hyclone) and Glutamax (Gibco). HepG2 cells were maintained in low-glucose DMEM with L-glutamine and sodium pyruvate (Gibco). One day before ionophore treatment, cells were passaged and plated in DMEM with Glutamax supplemented with 10% FBS on either poly D-lysine-coated (HEK 293T) or gelatin-coated (HepG2) sterile six-well Corning polystyrene plates. Cells were grown to 60−80% confluency prior to ionophore treatment.

Cellular Ionophore Treatment and ICP-MS Assays. Cells were washed twice with serum-free DMEM. Stock solutions of Cu(gtsm) or Gal-Cu(gtsm) (2 mM) were diluted in serum-free DMEM to a final ionophore concentration of 4 μM. A 2 mL amount of vehicle (0.2% DMSO in DMEM), 4 μM Cu(gtsm), or 4 μM Gal-Cu(gtsm) was then added to the six-well plates and incubated for three hours. For the galactose competition experiment, cells were washed twice with serum-free DMEM, then incubated with 2 mL of serum-free DMEM either with or without 1 M D-galactose (Sigma-Aldrich) for 15 min. A 4 μL amount of DMSO, 2 mM Cu(gtsm), or 10 mM Gal-Cu(gtsm) was diluted with 300 μL of cell media, which was then mixed back into each well. Cells were then incubated for one hour. Cells were then rinsed twice with ice-cold ethylenediamine tetraacetate (EDTA) (1 mM in 50 mM HEPES buffer, pH = 7.4) to remove cell-surface-bound copper and rinsed twice with ice-cold 50 mM HEPES buffer (pH = 7.4), followed by the addition of 215 μL of concentrated nitric acid (BDH Aristar Ultra). The plates were sealed with Parafilm and incubated on a shaker overnight. Samples (150 μL) were further diluted in 2 mL of 2% nitric acid (made freshly from concentrated nitric acid and Milli-Q water) in 15 mL tubes (Sarstedt) and analyzed on a Thermo Fisher iCAP Qc ICP mass spectrometer in kinetic energy discrimination (KED) mode against a standard curve of known copper and phosphorus concentrations (CMS-5, Inorganic Ventures), with Ga (20 μg/L, Inorganic Ventures) as an internal standard. Each experiment was carried out twice, and each condition was repeated in at least triplicate.

Animals. FVB-luc+ (FVB-Tg (CAG-luc,-GFP)L2G85Chco/J) mice were obtained from our in-house breeding colony. Mice were group housed on a 12:12 h light−dark cycle at 22 °C with free access to food and water. All animal studies were approved by and performed according to the guidelines of the Animal Care and Use Committee of the University of California, Berkeley.

General Animal Imaging Methods and Data Analysis. A Xenogen IVIS Spectrum instrument (Caliper Life Sciences) was used for bioluminescence imaging in all animal experiments, and image analysis was performed using the Living Image software. The total photon flux for each animal was determined by drawing a region of interest around the liver and integrating photon flux over the total imaging period (area under the curve). We selected our liver region of interest based on comparing the bioluminescence data *in vivo* and *ex vivo*, as described in our previous studies with the CCL-1 probe.[27] The same region of interest around the liver was applied to analyzing both the CCL-1 and D-Luc data. The data plotted in Figure 3A represent the ratio of CCL-1 integrated photon flux to basal D-luc integrated photon flux. Mice were anesthetized prior to injection and during imaging via inhalation of isoflurane. Isoflurane was purchased from Phoenix Pharmaceuticals, Inc. DMSO was purchased from Sigma-Aldrich, Dulbecco's phosphate-buffered saline (DPBS) was purchased from Gibco, and medical-grade oxygen was purchased from Praxair.

***In Vivo* Imaging with CCL-1.** FVB-luc+ mice were given i.p. injections of vehicle (50 μL 1:1 DMSO/DPBS), 3.46 mg/kg Cu(gtsm), or 7.26 mg/kg Gal-Cu(gtsm) under anesthesia with isoflurane. The ionophore concentrations were chosen to give an equivalent copper dose of 0.75 mg Cu/kg mouse at 0.6 mg Cu/mL vehicle. Six hours later, the same mice were anesthetized and subjected to scapular s.c. injection of CCL-1 (0.1 μmol in 50 μL DMSO/150 μL DPBS) or D-luciferin (0.1 μmol in 50 μL DMSO/150 μL DPBS). Five minutes after s.c. injection, mice were transferred to a Xenogen IVIS Spectrum and imaged for 40 min under 2% isoflurane anesthesia to characterize ionophore-treated liver signal response.

Tissue Harvesting and Serum Isolation. FVB-luc+ mice were heavily anesthetized, and blood was collected via cardiac puncture. Mice were immediately euthanized by cervical dislocation. Tissues were harvested, rinsed twice with DPBS, snap-frozen under liquid nitrogen, placed on dry ice in cryotubes, and stored at −80 °C until analysis. Serum was isolated by allowing blood samples to coagulate for 1 h at room temperature, centrifuging at 1500*g* for 15 min at 4 °C, then collecting the serum supernatant. Samples were aliquoted, snap-frozen, and stored at −80 °C until analysis.

Tissue Copper Analysis with ICP-MS. Portions of 20−100 mg of the harvested tissues were digested in concentrated nitric acid (100 mg tissue/mL HNO_3, BDH Aristar Ultra) at 95 °C for 2 h in 1.5 mL tubes (Sarstedt) with small holes poked in the caps with an 18G needle. After overnight incubation at room temperature, samples were diluted into freshly prepared 2% nitric acid and doped with a gallium internal standard (Inorganic Ventures, diluted from 1 ppm in 2% nitric acid to a 20 ppb final concentration). The copper content was determined by measuring ^{63}Cu using a Thermo Fisher iCAP-Qc ICP-MS in KED mode. Measurements were normalized to a standard curve of known copper concentrations doped with 20 ppb Ga. The standard curve was diluted from CMS-5 (Inorganic Ventures).

Liver Tissue Histology. FVB-luc+ mice were injected i.p. with vehicle (50 μL 1:1 DMSO/DPBS), Cu(gtsm), or Gal-Cu(gtsm) at a 0.75 mg Cu/kg mouse dose. After six hours, mice were euthanized with CO_2 asphyxiation followed by cervical dislocation, and liver tissue was extracted. Liver sections were fixed in a 10% formalin in PBS solution and sent to Histowiz Inc. (Brooklyn, NY, USA) for further processing and hematoxylin and eosin staining.

Liver Tissue Lysis. Frozen mouse livers were minced into 50 mg samples on dry ice and homogenized in ice-cold RIPA buffer (25 mM Tris·HCl pH 7.6, 150 mM NaCl, 1% NP-40, 1% sodium deoxycholate, 0.1% sodium dodecyl sulfate (SDS)) containing protease inhibitor cocktail with EDTA (Roche) at 100 mg/mL using a hand-held mechanical homogenizer. Homogenates were incubated on ice for 30 min and centrifuged at 12000*g* for 20 min at 4 °C. The soluble protein lysates were collected from underneath the upper lipid layer with a pipet and transferred to new tubes. Protein concentration was determined using a detergent-compatible Bradford Assay (Pierce).

Toxicity Assays of Liver Lysate and Serum. Liver lysate (TBARS assay via TCA method, Cayman Chemical) and serum (BUN assay, Invitrogen; ALT assay, Cayman Chemical) samples were processed according to the manufacturers' instructions; sample concentration was selected based on initial dilution screening to fall within a linear range of the standard curve. All samples were analyzed in triplicate.

Western Blot Analysis. Protein lysates were denatured in NuPAGE lithium dodecyl sulfate sample buffer (Invitrogen) containing 10% v/v β-mercaptoethanol as a reducing agent. The samples (20 μg for CCS, CTR1, ATP7B; 50 μg for MT) were resolved by SDS-PAGE using 15-well or 17-well NuPAGE 4−12% Bis-Tris gels (Invitrogen) with MES SDS running buffer (Invitrogen) with 10 μL of loading sample. Proteins were transferred to a polyvinylidene difluoride membrane (BioRad, Munich, Germany) with the use of the Trans-Blot Turbo transfer system (BioRad, Munich, Germany). The membranes were blocked in 5% nonfat dry milk in TBST buffer (10 mM Tris, pH 7.5, 100 mM NaCl, 0.1% Tween-20) for 1 h at room temperature. After blocking, the membranes were incubated at 4 °C overnight with primary antibodies diluted with TBST buffer containing 5% bovine serum albumin (BSA). The anti-ATP7B (NB100-360, Novus Biologics) and anti-metallothionein (sc-11377, Santa Cruz Biotechnology) were used at 1:250 dilution. The anti-CTR1 antibody (13086, Cell Signaling Technology) was used at 1:1000 dilution. The anti-CCS (sc-20141, Santa Cruz Biotechnology) was used at 1:500 dilution. The membranes were washed three times for 5 min in TBST and incubated for 1 h at room temperature with horseradish peroxidase (HRP)-conjugated anti-rabbit IgG secondary antibody (sc-2004,

DOI: 10.1021/jacs.8b08014
J. Am. Chem. Soc. 2018, 140, 13764−13774

Santa Cruz Biotechnology) at a 1:2000 dilution in TBST containing 5% BSA. The membranes were washed five times for 5 min in TBST, then visualized using enhanced chemiluminescence (Western Lighting Plus for visualizing CCS and ATP7B, PerkinElmer; Western Clarity Max for visualizing CTR1 and MT, Bio-Rad) recorded on a BioRad GelDoc imaging station. β-Actin was probed to determine equal loading using anti-β-actin (sc-69879, Santa Cruz Biotechnology) and AlexaFluor 647-conjugated anti-mouse IgG (A31571, Molecular Probes) antibodies at 1:5000 and 1:2500 dilutions, respectively, with visualization using fluorescence recorded on a BioRad GelDoc imaging station.

■ ASSOCIATED CONTENT

Supporting Information

The Supporting Information is available free of charge on the ACS Publications website at DOI: 10.1021/jacs.8b08014.

Additional experimental details (PDF)

■ AUTHOR INFORMATION

Corresponding Authors

*astahl@berkeley.edu

*chrischang@berkeley.edu

ORCID

Timothy A. Su: 0000-0001-5934-3292

Marie C. Heffern: 0000-0001-7501-2741

Christopher J. Chang: 0000-0001-5732-9497

Present Address

#Department of Chemistry, University of California, Davis, California 95616, United States.

Notes

The authors declare no competing financial interest.

■ ACKNOWLEDGMENTS

We thank Alison Killilea and Carissa Tasto at UC Berkeley's Cell Culture Facility for expert technical assistance. We thank National Institutes of Health (NIH) (Grants GM79465 and ES4705 to C.J.C. and Grant R01CA221916 to A.S.) for support. T.A.S. thanks the NIH Ruth L. Kirschstein National Research Service Award (Grant F32 GM122248) for support and Dr. Lakshmi Krishnamoorthy for helpful discussions. W.C. was supported by the UC Berkeley Amgen Scholars Program. M.C.H. was supported by the University of California President's Postdoctoral Program. T.D. was partially supported by NIH Chemical Biology Training Grant T32 GM066698. C.J.C. is an Investigator with the Howard Hughes Medical Institute.

■ REFERENCES

(1) Lippard, S. J.; Berg, J. M. *Principles of Bioinorganic Chemistry*; University Science Books: Mill Valley, CA, 1994.

(2) Ferguson-Miller, S.; Babcock, G. T. *Chem. Rev.* **1996**, *96*, 2889.

(3) McCord, J. M.; Fridovich, I. *J. Biol. Chem.* **1969**, *244*, 6049.

(4) Hart, P. J.; Balbirnie, M. M.; Ogihara, N. L.; Nersissian, A. M.; Weiss, M. S.; Valentine, J. S.; Eisenberg, D. *Biochemistry* **1999**, *38*, 2167.

(5) Prigge, S. T.; Mains, R. E.; Eipper, B. A.; Amzel, L. M. *Cell. Mol. Life Sci.* **2000**, *57*, 1236.

(6) Friedman, S.; Kaufman, S. *J. Biol. Chem.* **1966**, *241*, 2256.

(7) Solomons, N. W. *J. Am. Coll. Nutr.* **1985**, *4*, 83.

(8) Bost, M.; Houdart, S.; Oberli, M.; Kalonji, E.; Huneau, J. F.; Margaritis, I. *J. Trace Elem. Med. Biol.* **2016**, *35*, 107.

(9) Brady, D. C.; Crowe, M. S.; Turski, M. L.; Hobbs, G. A.; Yao, X.; Chaikuad, A.; Knapp, S.; Xiao, K.; Campbell, S. L.; Thiele, D. J.; Counter, C. M. *Nature* **2014**, *509*, 492.

(10) Turski, M. L.; Brady, D. C.; Kim, H. J.; Kim, B.-E.; Nose, Y.; Counter, C. M.; Winge, D. R.; Thiele, D. J. *Mol. Cell. Biol.* **2012**, *32*, 1284.

(11) Dodani, S. C.; Firl, A.; Chan, J.; Nam, C. I.; Aron, A. T.; Onak, C. S.; Ramos-Torres, K. M.; Paek, J.; Webster, C. M.; Feller, M. B.; Chang, C. J. *Proc. Natl. Acad. Sci. U. S. A.* **2014**, *111*, 16280.

(12) Krishnamoorthy, L.; Cotruvo, J. A.; Chan, J.; Kaluarachchi, H.; Muchenditsi, A.; Pendyala, V. S.; Jia, S.; Aron, A. T.; Ackerman, C. M.; Vander Wal, M. N.; Guan, T.; Smaga, L. P.; Farhi, S. L.; New, E. J.; Lutsenko, S.; Chang, C. J. *Nat. Chem. Biol.* **2016**, *12*, 586.

(13) Vulpe, C.; Levinson, B.; Whitney, S.; Packman, S.; Gitschier, J. *Nat. Genet.* **1993**, *3*, 7.

(14) Roberts, B. R.; Tainer, J. A.; Getzoff, E. D.; Malencik, D. A.; Anderson, S. R.; Bomben, V. C.; Meyers, K. R.; Karplus, P. A.; Beckman, J. S. *J. Mol. Biol.* **2007**, *373*, 877.

(15) McAllum, E. J. M. C.; Lim, N. K.; Hickey, J. L.; Paterson, B. M.; Donnelly, P. S.; Li, Q.; Liddell, J. R.; Barnham, K. J.; White, A. R.; Crouch, P. J. *Amyotrophic Lateral Scler. Frontotemporal Degener.* **2013**, *14*, 586.

(16) Bush, A. I. *J. Alzheimer's Dis.* **2008**, *15*, 223.

(17) Hayne, D. J.; Lim, S.; Donnelly, P. S. *Chem. Soc. Rev.* **2014**, *43*, 6701.

(18) Perez, L. R.; Franz, K. J. *Dalton Trans.* **2010**, *39*, 2177.

(19) Elsherif, L.; Ortines, R. V.; Saari, J. T.; Kang, Y. J. *Exp. Biol. Med.* **2003**, *228*, 811.

(20) Klevay, L. M. *Biol. Trace Elem. Res.* **1983**, *5*, 245.

(21) Stättermayer, A. F.; Traussnigg, S.; Aigner, E.; Kienbacher, C.; Huber-Schönauer, U.; Steindl-Munda, P.; Stadlmayr, A.; Wrba, F.; Trauner, M.; Datz, C.; Ferenci, P. *J. Trace Elem. Med. Biol.* **2017**, *39*, 100.

(22) Aigner, E.; Strasser, M.; Haufe, H.; Sonnweber, T.; Hohla, F.; Stadlmayr, A.; Solioz, M.; Tilg, H.; Patsch, W.; Weiss, G.; Stickel, F.; Datz, C. *Am. J. Gastroenterol.* **2010**, *105*, 1978.

(23) Aigner, E.; Weiss, G.; Datz, C. *World J. Hepatol.* **2014**, *7*, 177.

(24) Huster, D.; Purnat, T. D.; Burkhead, J. L.; Ralle, M.; Fiehn, O.; Stuckert, F.; Olson, N. E.; Teupser, D.; Lutsenko, S. *J. Biol. Chem.* **2007**, *282*, 8343.

(25) Burkhead, J. L.; Lutsenko, S. *Lipid Metab.* **2013**, 39.

(26) Morrell, A.; Tallino, S.; Yu, L.; Burkhead, J. L. *IUBMB Life* **2017**, *69*, 263.

(27) Heffern, M. C.; Park, H. M.; Au-Yeung, H. Y.; Van de Bittner, G. C.; Ackerman, C. M.; Stahl, A.; Chang, C. J. *Proc. Natl. Acad. Sci. U. S. A.* **2016**, *113*, 14219.

(28) Weekley, C. M.; He, C. *Curr. Opin. Chem. Biol.* **2017**, *37*, 26.

(29) Helsel, M. E.; Franz, K. J. *Dalt. Trans.* **2015**, *44*, 8760.

(30) Sarkar, B.; Lingertat-Walsh, K.; Clarke, J. T. R. *J. Pediatr.* **1993**, *123*, 828.

(31) Crouch, P. J.; Hung, L. W.; Adlard, P. A.; Cortes, M.; Lal, V.; Filiz, G.; Perez, K. A.; Nurjono, M.; Caragounis, A.; Du, T.; Laughton, K.; Volitakis, I.; Bush, A. I.; Li, Q.-X.; Masters, C. L.; Cappai, R.; Cherny, R. A.; Donnelly, P. S.; White, A. R.; Barnham, K. J. *Proc. Natl. Acad. Sci. U. S. A.* **2009**, *106*, 381.

(32) Donnelly, P. S.; Liddell, J. R.; Lim, S.; Paterson, B. M.; Cater, M. A.; Savva, M. S.; Mot, A. I.; James, J. L.; Trounce, I. A.; White, A. R.; Crouch, P. J. *Proc. Natl. Acad. Sci. U. S. A.* **2012**, *109*, 47.

(33) Paterson, B. M.; Donnelly, P. S. *Chem. Soc. Rev.* **2011**, *40*, 3005.

(34) Cherny, R. A.; Atwood, C. S.; Xilinas, M. E.; Gray, D. N.; Jones, W. D.; McLean, C. A.; Barnham, K. J.; Volitakis, I.; Fraser, F. W.; Kim, Y. S.; Huang, X.; Goldstein, L. E.; Moir, R. D.; Lim, J. T.; Beyreuther, K.; Zheng, H.; Tanzi, R. E.; Masters, C. L.; Bush, A. I. *Neuron* **2001**, *30*, 665.

(35) Halliwell, B.; Gutteridge, J. M. *Biochem. J.* **1984**, *219*, 1.

(36) Cater, M. A.; Pearson, H. B.; Wolyniec, K.; Klaver, P.; Bilandzic, M.; Paterson, B. M.; Bush, A. I.; Humbert, P. O.; La Fontaine, S.; Donnelly, P. S.; Haupt, Y. *ACS Chem. Biol.* **2013**, *8*, 1621.

DOI: 10.1021/jacs.8b08014
J. Am. Chem. Soc. 2018, 140, 13764−13774

(37) Shimada, K.; Reznik, E.; Stokes, M. E.; Krishnamoorthy, L.; Bos, P. H.; Song, Y.; Quartararo, C. E.; Pagano, N. C.; Carpizo, D. R.; deCarvalho, A. C.; Lo, D. C.; Stockwell, B. R. *Cell Chem. Biol.* **2018**, *25*, 585.
(38) John, E. K.; Green, M. A. *J. Med. Chem.* **1990**, *33*, 1764.
(39) Torres, J. B.; Andreozzi, E. M.; Dunn, J. T.; Siddique, M.; Szanda, I.; Howlett, D. R.; Sunassee, K.; Blower, P. J. *J. Nucl. Med.* **2016**, *57*, 109.
(40) Younossi, Z.; Anstee, Q. M.; Marietti, M.; Hardy, T.; Henry, L.; Eslam, M.; George, J.; Bugianesi, E. *Nat. Rev. Gastroenterol. Hepatol.* **2018**, *15*, 11.
(41) Byrne, C. D.; Targher, G. *J. Hepatol.* **2015**, *62*, S47.
(42) Leung, T. M.; Nieto, N. *J. Hepatol.* **2013**, *58*, 395.
(43) Wu, X.; Zhang, L.; Gurley, E.; Studer, E.; Shang, J.; Wang, T.; Wang, C.; Yan, M.; Jiang, Z.; Hylemon, P. B.; Sanyal, A. J.; Pandak, W. M.; Zhou, H. *Hepatology* **2008**, *47*, 1905.
(44) Blaby-Haas, C. E.; Merchant, S. S. *J. Biol. Chem.* **2014**, *289*, 28129.
(45) Polishchuk, E. V.; Polishchuk, R. S. *Metallomics* **2016**, *8*, 853.
(46) Polishchuk, E. V.; Concilli, M.; Iacobacci, S.; Chesi, G.; Pastore, N.; Piccolo, P.; Paladino, S.; Baldantoni, D.; Van Ijzendoorn, S. C. D.; Chan, J.; Chang, C. J.; Amoresano, A.; Pane, F.; Pucci, P.; Tarallo, A.; Parenti, G.; Brunetti-Pierri, N.; Settembre, C.; Ballabio, A.; Polishchuk, R. S. *Dev. Cell* **2014**, *29*, 686.
(47) D'Souza, A. A.; Devarajan, P. V. *J. Controlled Release* **2015**, *203*, 126.
(48) Mamidyala, S. K.; Dutta, S.; Chrunyk, B. A.; Préville, C.; Wang, H.; Withka, J. M.; McColl, A.; Subashi, T. A.; Hawrylik, S. J.; Griffor, M. C.; Kim, S.; Pfefferkorn, J. A.; Price, D. A.; Menhaji-Klotz, E.; Mascitti, V.; Finn, M. G. *J. Am. Chem. Soc.* **2012**, *134*, 1978.
(49) Julyan, P. J.; Seymour, L. W.; Ferry, D. R.; Daryani, S.; Boivin, C. M.; Doran, J.; David, M.; Anderson, D.; Christodoulou, C.; Young, A. M.; Hesslewood, S.; Kerr, D. J. *J. Controlled Release* **1999**, *57*, 281.
(50) Rensen, P. C. N.; Van Leeuwen, S. H.; Sliedregt, L. A. J. M.; Van Berkel, T. J. C.; Biessen, E. A. L. *J. Med. Chem.* **2004**, *47*, 5798.
(51) Lee, K.; Rafi, M.; Wang, X.; Aran, K.; Feng, X.; Lo Sterzo, C.; Tang, R.; Lingampalli, N.; Kim, H. J.; Murthy, N. *Nat. Mater.* **2015**, *14*, 701.
(52) Nair, J. K.; Willoughby, J. L. S.; Chan, A.; Charisse, K.; Alam, M. R.; Wang, Q.; Hoekstra, M.; Kandasamy, P.; Kel'in, A. V.; Milstein, S.; Taneja, N.; O'Shea, J.; Shaikh, S.; Zhang, L.; van der Sluis, R. J.; Jung, M. E.; Akinc, A.; Hutabarat, R.; Kuchimanchi, S.; Fitzgerald, K.; Zimmermann, T.; van Berkel, T. J. C.; Maier, M. A.; Rajeev, K. G.; Manoharan, M. *J. Am. Chem. Soc.* **2014**, *136*, 16958.
(53) Rozema, D. B.; Lewis, D. L.; Wakefield, D. H.; Wong, S. C.; Klein, J. J.; Roesch, P. L.; Bertin, S. L.; Reppen, T. W.; Chu, Q.; Blokhin, A. V.; Hagstrom, J. E.; Wolff, J. A. *Proc. Natl. Acad. Sci. U. S. A.* **2007**, *104*, 12982.
(54) Rouet, R.; Thuma, B. A.; Roy, M. D.; Lintner, N. G.; Rubitski, D. M.; Finley, J. E.; Wisniewska, H. M.; Mendonsa, R.; Hirsh, A.; de Oñate, L.; Compte Barrón, J.; McLellan, T. J.; Bellenger, J.; Feng, X.; Varghese, A.; Chrunyk, B. A.; Borzilleri, K.; Hesp, K. D.; Zhou, K.; Ma, N.; Tu, M.; Dullea, R.; McClure, K. F.; Wilson, R. C.; Liras, S.; Mascitti, V.; Doudna, J. A. *J. Am. Chem. Soc.* **2018**, *140*, 6596.
(55) Pujol, A. M.; Cuillel, M.; Renaudet, O.; Lebrun, C.; Charbonnier, P.; Cassio, D.; Gateau, C.; Dumy, P.; Mintz, E.; Delangle, P. *J. Am. Chem. Soc.* **2011**, *133*, 286.
(56) Pujol, A. M.; Cuillel, M.; Jullien, A. S.; Lebrun, C.; Cassio, D.; Mintz, E.; Gateau, C.; Delangle, P. *Angew. Chem., Int. Ed.* **2012**, *51*, 7445.
(57) Stokmaier, D.; Khorev, O.; Cutting, B.; Born, R.; Ricklin, D.; Ernst, T. O. G.; Böni, F.; Schwingruber, K.; Gentner, M.; Wittwer, M.; Spreafico, M.; Vedani, A.; Rabbani, S.; Schwardt, O.; Ernst, B. *Bioorg. Med. Chem.* **2009**, *17*, 7254.
(58) Choi, J. S.; Braymer, J. J.; Nanga, R. P. R.; Ramamoorthy, A.; Lim, M. H. *Proc. Natl. Acad. Sci. U. S. A.* **2010**, *107*, 21990.
(59) Sharma, A. K.; Pavlova, S. T.; Kim, J.; Finkelstein, D.; Hawco, N. J.; Rath, N. P.; Kim, J.; Mirica, L. M. *J. Am. Chem. Soc.* **2012**, *134*, 6625.
(60) Haas, K. L.; Franz, K. J. *Chem. Rev.* **2009**, *109*, 4921.
(61) Bica, L.; Liddell, J. R.; Donnelly, P. S.; Duncan, C.; Caragounis, A.; Volitakis, I.; Paterson, B. M.; Cappai, R.; Grubman, A.; Camakaris, J.; Crouch, P. J.; White, A. R. *PLoS One* **2014**, *9*.e90070
(62) Crouch, P. J.; Barnham, K. J. *Acc. Chem. Res.* **2012**, *45*, 1604.
(63) Palanimuthu, D.; Shinde, S. V.; Somasundaram, K.; Samuelson, A. G. *J. Med. Chem.* **2013**, *56*, 722.
(64) Xiao, Z.; Donnelly, P. S.; Zimmermann, M.; Wedd, A. G. *Inorg. Chem.* **2008**, *47*, 4338.
(65) Price, K. A.; Crouch, P. J.; Volitakis, I.; Paterson, B. M.; Lim, S.; Donnelly, P. S.; White, A. R. *Inorg. Chem.* **2011**, *50*, 9594.
(66) Dearling, J. L. J.; Lewis, J. S.; Mullen, G. E. D.; Welch, M. J.; Blower, P. J. *JBIC, J. Biol. Inorg. Chem.* **2002**, *7*, 249.
(67) Klayman, D. L.; Lin, A. J. *Org. Prep. Proced. Int.* **1984**, *16*, 79.
(68) Brett, M. P.; John, A. K.; Denis, B. S.; Jonathan, M. W.; Donnelly, P. S. *Inorg. Chem.* **2010**, *49*, 1884.
(69) Barnham, K. J.; Donnelly, P. S.; White, A. R. Metal delivery agents and therapeutic uses of the same. PCT/AU2007/001792, 2007.
(70) Wang, W.; Jin, C.; Guo, L.; Liu, Y.; Wan, Y.; Wang, X.; Li, L.; Zhao, W.; Wang, P. G. *Chem. Commun.* **2011**, *47*, 11240.
(71) Andrés, A.; Rosés, M.; Ràfols, C.; Bosch, E.; Espinosa, S.; Segarra, V.; Huerta, J. M. *Eur. J. Pharm. Sci.* **2015**, *76*, 181.
(72) Carter, K. P.; Young, A. M.; Palmer, A. E. *Chem. Rev.* **2014**, *114*, 4564.
(73) Xiao, T.; Ackerman, C. M.; Carroll, E. C.; Jia, S.; Hoagland, A.; Chan, J.; Thai, B.; Liu, C. S.; Isacoff, E. Y.; Chang, C. J. *Nat. Chem. Biol.* **2018**, *14*, 655.
(74) Bremer, P. T.; Pellett, S.; Carolan, J. P.; Tepp, W. H.; Eubanks, L. M.; Allen, K. N.; Johnson, E. A.; Janda, K. D. *J. Am. Chem. Soc.* **2017**, *139*, 7264.
(75) Li, Y.; Huang, G.; Diakur, J.; Wiebe, L. I. *Curr. Drug Delivery* **2008**, *5*, 299.
(76) Zachary, J. F. *Pathologic Basis of Veterinary Disease*;, 6th ed.; Elsevier: St Louis, MO, 2017.
(77) Tardito, S.; Bassanetti, I.; Bignardi, C.; Elviri, L.; Tegoni, M.; Mucchino, C.; Bussolati, O.; Franchi-Gazzola, R.; Marchiò, L. *J. Am. Chem. Soc.* **2011**, *133*, 6235.
(78) Ohrvik, H.; Nose, Y.; Wood, L. K.; Kim, B.-E.; Gleber, S.-C.; Ralle, M.; Thiele, D. J. *Proc. Natl. Acad. Sci. U. S. A.* **2013**, *110*, E4279.
(79) Harada, M.; Sakisaka, S.; Terada, K.; Kimura, R.; Kawaguchi, T.; Koga, H.; Taniguchi, E.; Sasatomi, K.; Miura, N.; Suganuma, T.; Fujita, H.; Furuta, K.; Tanikawa, K.; Sugiyama, T.; Sata, M. *Gastroenterology* **2000**, *118*, 921.
(80) Alsaggar, M.; Liu, D. *J. Drug Target.* **2018**, *26*, 385.
(81) Denoyer, D.; Pearson, H. B.; Clatworthy, S. A. S.; Smith, Z. M.; Francis, P. S.; Llanos, R. M.; Volitakis, I.; Phillips, W. A.; Meggyesy, P. M.; Masaldan, S.; Cater, M. A. *Oncotarget* **2016**, *7*, 37064.
(82) Skrott, Z.; Mistrik, M.; Andersen, K. K.; Friis, S.; Majera, D.; Gursky, J.; Ozdian, T.; Bartkova, J.; Turi, Z.; Moudry, P.; Kraus, M.; Michalova, M.; Vaclavkova, J.; Dzubak, P.; Vrobel, I.; Pouckova, P.; Sedlacek, J.; Miklovicova, A.; Kutt, A.; Li, J.; Mattova, J.; Driessen, C.; Dou, Q. P.; Olsen, J.; Hajduch, M.; Cvek, B.; Deshaies, R. J.; Bartek, J. *Nature* **2017**, *552*, 194.
(83) Brun, M. A.; Tan, K. T.; Griss, R.; Kielkowska, A.; Reymond, L.; Johnsson, K. *J. Am. Chem. Soc.* **2012**, *134*, 7676.

DOI: 10.1021/jacs.8b08014
J. Am. Chem. Soc. 2018, 140, 13764−13774